Structure
Short Article

Structural Studies of Wnts and Identification of an LRP6 Binding Site

Matthew Ling-Hon Chu,[1] Victoria E. Ahn,[1,4] Hee-Jung Choi,[1,2] Danette L. Daniels,[1,5] Roel Nusse,[3] and William I. Weis[1,*]
[1]Departments of Structural Biology and Molecular and Cellular Physiology, Stanford University School of Medicine, Stanford, CA 94305, USA
[2]Department of Biological Sciences, Seoul National University, Seoul, 151-747, South Korea
[3]Department of Developmental Biology and Howard Hughes Medical Institute, Stanford University School of Medicine, Stanford, CA 94305, USA
[4]Present address: Cocrystal Discovery, Mountain View, CA 94043, USA
[5]Present address: Promega, Madison, WI 53711, USA
*Correspondence: bill.weis@stanford.edu
http://dx.doi.org/10.1016/j.str.2013.05.006

SUMMARY

Wnts are secreted growth factors that have critical roles in cell fate determination and stem cell renewal. The Wnt/β-catenin pathway is initiated by binding of a Wnt protein to a Frizzled (Fzd) receptor and a coreceptor, LDL receptor-related protein 5 or 6 (LRP5/6). We report the 2.1 Å resolution crystal structure of a *Drosophila* WntD fragment encompassing the N-terminal domain and the linker that connects it to the C-terminal domain. Differences in the structures of WntD and *Xenopus* Wnt8, including the positions of a receptor-binding β hairpin and a large solvent-filled cavity in the helical core, indicate conformational plasticity in the N-terminal domain that may be important for Wnt-Frizzled specificity. Structure-based mutational analysis of mouse Wnt3a shows that the linker between the N- and C-terminal domains is required for LRP6 binding. These findings provide important insights into Wnt function and evolution.

INTRODUCTION

Wnt proteins constitute a large family of growth factors that regulate diverse aspects of embryonic development and tissue homeostasis. Wnts bind to specific receptors on the cell surface and can trigger various signaling pathways. In the Wnt/β-catenin pathway, Wnts bind to a Frizzled (Fzd) receptor and to one of the LRP5 or LRP6 receptors, which leads to stabilization of the transcriptional coactivator β-catenin and activation of target genes (MacDonald et al., 2009). There are multiple Wnt proteins encoded in metazoan genomes; for example, 19 Wnt genes are present in the human genome.

Wnts are 350- to 400-residue-long secreted proteins that feature a conserved pattern of 22–24 cysteine residues. Most Wnts are posttranlationally modified by glycosylation and fatty acylation. Whereas the sites of glycosylation are not conserved, lipid modification of a conserved serine residue (Ser209 of Wnt3a) is indispensable for intracellular processing, secretion, and activity of almost all Wnt proteins (Takada et al., 2006). An exception is *Drosophila melanogaster* WntD, which inhibits nuclear accumulation of Dorsal/NF-κB during embryonic dorsal/ventral patterning and in the adult innate immune response and also regulates migration of embryonic primordial germ cells to the gonad (Gordon et al., 2005; Ganguly et al., 2005; McElwain et al., 2011). WntD is not lipidated or glycosylated (Gordon et al., 2005; Ganguly et al., 2005; Ching et al., 2008). It does not signal through the canonical Wnt/β-catenin pathway (Gordon et al., 2005), but may interact with Fzd4 (McElwain et al., 2011).

The recently published crystal structure of *Xenopus* Wnt8 (XWnt8) bound to the Fzd8 cysteine-rich domain (CRD) shows that Wnt proteins comprise two structural subdomains: a larger N-terminal domain (NTD) comprising a six-helix core and two protruding β-hairpins, one of which bears the lipid; and a C-terminal domain (CTD) that is a cytokine-like hairpin loop (Janda et al., 2012; Bazan et al., 2012). The lipid interacts with Fzd, as do residues on the tip of the CTD hairpin. A linking peptide of variable length and sequence among Wnt proteins connects the two domains; the N- and C-terminal ends of the linker feature conserved residues that form the NTD-CTD interface.

Here, we describe the high-resolution crystal structure of an uncomplexed *Drosophila* WntD fragment comprising the NTD and linker region. Comparison with the XWnt8 structure suggests features of conformational plasticity that may be important for the ability of Wnt proteins to interact with multiple receptors. We also show that the linker connecting the N- and C-terminal domains of Wnt proteins is required for binding to LRP6.

RESULTS

Crystal Structure of Uncomplexed WntD N-Terminal Domain-Linker

The hydrophobic nature imparted by lipid modification has hampered structural analyses of uncomplexed Wnt proteins. *Drosophila* WntD lacks lipid modification or N-linked glycosylation (Ching et al., 2008) and can be expressed at relatively high levels, so we chose this protein for structural studies. Extensive crystallization screens of full length WntD produced only poorly diffracting crystals, and we could not detect binding to purified *Drosophila* Fzd4 CRD, eliminating cocrystallization with this putative receptor as an option. We therefore sought to produce

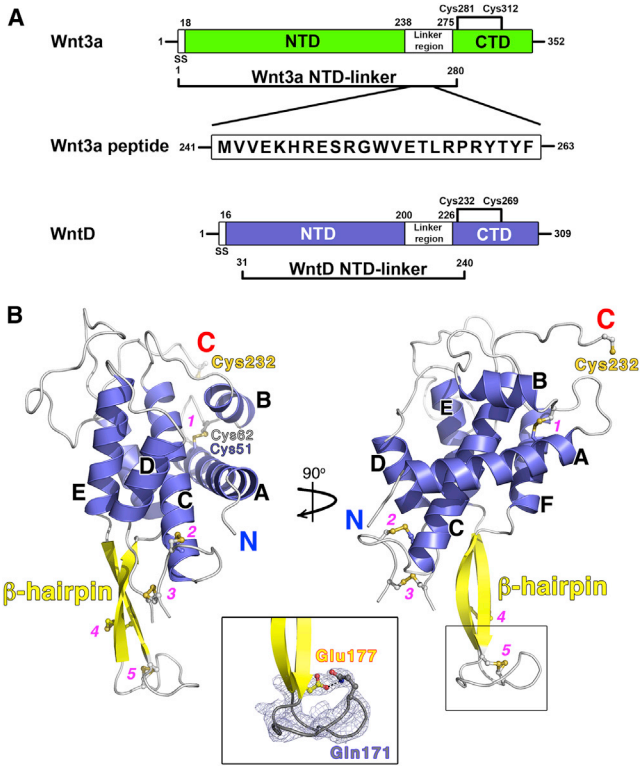

Figure 1. Crystal Structure of the *Drosophila* WntD NTD-Linker

(A) Primary structures of WntD and Wnt3a. An attempt to produce a C-terminal truncated Wnt3a construct (Wnt3a NTD-linker) equivalent to the dominant negative mutants of mouse Wnt1 or *Xenopus* Wnt8 was not successful (see also Figure S1), probably due to the unpaired Cys281 forms a disulfide bond in the full-length protein. Truncating Wnt3a just before Cys281 yielded a secreted protein that could be purified (see also Figures S2B and S4A). The Wnt3a linker peptide used in this study is also shown. WntD Cys232 is a conserved cysteine that normally forms a disulfide bond with another conserved cysteine Cys269 within the Wnt CTD, but is unpaired in the crystallized WntD NTD-linker construct. SS, signal sequence.

(B) Two orthogonal views of the WntD NTD-linker structure. α helices A–F are shown in blue and the β hairpin in yellow. The five disulfide bridges are depicted as yellow sticks. The Cys51-Cys62 disulfide pair and the free Cys232 at the C terminus are labeled. The inset shows the tip of the β hairpin that contains the conserved acylated serine in other Wnt family members, but is a glutamine in WntD (Glu171). A fist-like structure of the tip of the β hairpin is observed in WntD (dark gray) and is stabilized by a hydrogen bond (dashed line) between Gln171 and Glu177 (sticks), as evidenced by the visible electron density (gray mesh, $2F_o$-F_c map contoured at 0.9 σ).

Table 1. X-Ray Crystallography Data Collection and Refinement Statistics

Data Collection	
Space group	$P4_1$
Unit Cell Dimensions	
a, *b*, *c* (Å)	59.6, 59.6, 67.0
α, β, γ (°)	90, 90, 90
Resolution (Å)	35.7–2.12 (2.24–2.12)
Unique reflections	13,301
$CC_{1/2}$[a]	1.0 (0.82)
R_{merge}[b]	0.076 (1.58)
$\langle I \rangle / \langle \sigma I \rangle$	23.2 (2.2)
Completeness (%)	99.9 (99.9)
Multiplicity	13.5 (13.8)
Refinement	
PDB code	4KRR
Resolution (Å)	29.8–2.12
No. reflections work/test set	13,272/654
R_{work}/R_{free}[c]	0.179/0.204
Number of Atoms	
Protein	1,465
Glycerol	24
Water	72
Sodium ion	1
Average B-Factors (Å^2)	
Protein	55.4
Glycerol	79.8
Water	48.0
Sodium ion	80.1
Rmsd	
Bond lengths (Å)	0.002
Bond angles (°)	0.56
Ramachandran Plot (%)[d]	
Favored regions	95.8
Additional allowed regions	4.2
Outliers	0

Values in parentheses are for highest-resolution shell.

[a]As defined in Scala (Evans, 2006).

[b]$R_{merge} = \Sigma_h \Sigma_i |I_i(h) - \langle I(h) \rangle| / \Sigma_h \Sigma_i I_i(h)$, where $I_i(h)$ is the I^{th} measurement of reflection h, and $\langle I(h) \rangle$ is the weighted mean of all measurements of h.

[c]$R = \Sigma_h |F_{obs}(h) - F_{calc}(h)| / \Sigma_h |F_{obs}(h)|$. R_{work} and R_{free} were calculated using the working and test reflection sets, respectively.

[d]As defined in MolProbity (Chen et al., 2010).

a truncated version for crystallographic studies. Truncation mutants of *Drosophila Wingless* (*Wg*), mouse Wnt1 or *Xenopus* Wnt8 lacking the C-terminal cytokine-like domain (Figure S1 available online) are secreted and can antagonize Wnt signaling (Couso and Martinez Arias, 1994; Bejsovec and Wieschaus, 1995; Hoppler et al., 1996; Wu and Nusse, 2002), which we could also demonstrate with purified Wnt3a protein (Figures 1A, S2A, and S2B). These data indicate that the NTD can fold separately and presumably antagonizes signaling by binding to either or both Fzd and LRP5/6 receptors independently of the CTD, so we designed a similar WntD NTD construct for crystallization.

Limited proteolysis of full-length WntD confirmed the stability of this fragment (Figure S2C) which, when compared to the structure of XWnt8 (Janda et al., 2012), spans the N-terminal subdomain and the linker region that connects this domain to the smaller C-terminal cytokine-like domain. We crystallized this construct, designated WntD NTD-linker, and determined its structure at 2.1 Å resolution (Table 1).

The WntD NTD-linker is composed of six α helices (labeled A to F) and two long antiparallel β strands in a β hairpin that link helices E and F. The overall architecture of the WntD NTD-linker is similar to that of Fzd-bound XWnt8, consistent with the 27% sequence identity between the two proteins

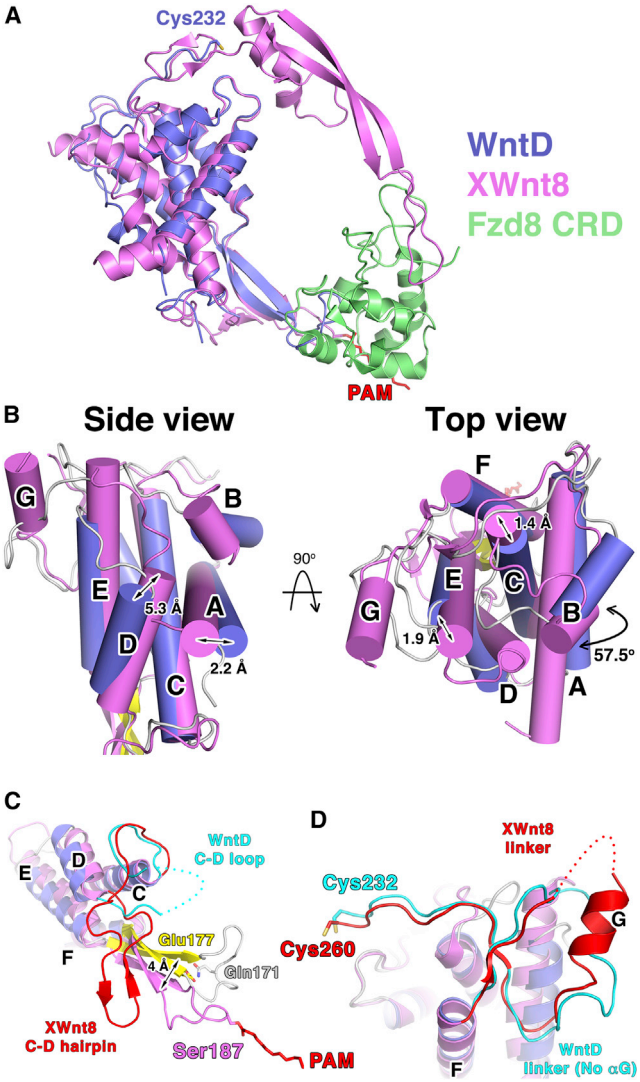

Figure 2. Comparison of *Drosophila* WntD and *Xenopus* Wnt8 Crystal Structures

(A) Superposition of WntD (blue) and the XWnt8 (magenta)-Fzd8 CRD (green) complex. The crystal structure of WntD in the present study contains the N-terminal domain and the linker that connects it to the C-terminal domain, which ends at Cys232 (blue stick). The lipid at Ser187 of XWnt8 that makes extensive contact with Fzd8 CRD is labeled as palmitoleic acid modification (PAM, red stick).

(B) Cylinder representation of superimposed NTD-linker regions of WntD (blue) and XWnt8 (magenta) viewed from the side and the top. The root mean square deviation between the two structures is 2.0 Å for 168 Cα atoms. The less compact core of WntD is evident by the outward displacement of helices A, C, D, and E relative to those of XWnt8. Helix B of the two structures also differ by a rotation of ~58°.

(C) Conformations of the β hairpins. The tip of the XWnt8 hairpin that connects helices E and F adopts an extended conformation with the lipid-modified Ser187 (magenta stick with red lipid, labeled PAM) extending from the tip, whereas the equivalent loop of WntD adopts a fist-like structure. WntD Gln171, the equivalent residue of XWnt8 Ser187, is shown in light-gray stick, and its interacting residue WntD Glu177 is depicted as yellow stick. The 4 Å displacement of the antiparallel β strands relative to those of XWnt8 is highlighted. XWnt8 contains a second β hairpin between helices C and D (XWnt8 C–D hairpin, red, residues 108–135), whereas the equivalent loop in WntD (WntD C–D loop, cyan, residues 105–113, 120–124) is much shorter and partially disordered in the structure (dotted cyan line).

(D) Linker region between the N-terminal and C-terminal domains of Wnts. The loop that connects the interface motifs is partially disordered in XWnt8 (dotted red line), but includes helix G (XWnt8 linker, red, residues 216–221, 235–260). The equivalent loop of WntD is well ordered (WntD linker, cyan, residues 200–232) and follows a similar path as that of XWnt8 toward to C terminus but does not contain the α-helix G. The last residue of WntD NTD-linker Cys232 and the equivalent Cys260 of XWnt8 are shown in sticks.

(Figures 2A and S1). Ten of the 11 conserved cysteine residues in the NTD-linker form five disulfide bridges that stabilize loops between helices A and B, helices C and D, and the β hairpin (Figure 1B). As observed in the XWnt8 structure, Cys51 in helix A, equivalent to residue XWnt8 Cys55 and mouse Wnt3a Cys77, forms a disulfide bond with Cys62 in the interhelical loop (Figure 1B), confirming that this conserved cysteine is not post-translationally modified (Janda et al., 2012). The last residue visible in the WntD NTD-linker structure is Cys232, which normally forms a disulfide bond within the CTD. Although the CTD is absent the present structure and Cys232 is unpaired in the crystallized construct, its position is virtually the same as its equivalent in XWnt8 (Figure 2D). This indicates that the structure observed here is likely a low energy, stable conformation.

Structural Differences between WntD and XWnt8 at the β Hairpin and Helical Core

Virtually all Wnt proteins feature a conserved serine at the tip of the β hairpin that connects helices E and F. This residue is modified by fatty acylation as shown for Wnt3a (Ser209) (Takada et al., 2006) and XWnt8 (Ser187) (Janda et al., 2012). WntD, however, contains a glutamine rather than a serine in this position (Figure S1). The tip of the WntD hairpin folds back to create a fist-like structure stabilized by a hydrogen bond between the Gln171 side chain and Glu177 (Figures 1B and 2C). In contrast, the tip of the XWnt8 hairpin adopts an extended conformation stabilized by the lipid-in-groove contact with the Fzd8 CRD (Figure 2C). Small displacements of the antiparallel β strands and helix E relative to their counterparts in XWnt8 can also be observed (Figures 2B and 2C). The position and conformation of E–F WntD hairpin might be stabilized in part by contacts with another molecule in the crystal lattice (Figure S3). XWnt8 also contains a second hairpin between helices C and D that forms a β sheet structure with the E–F hairpin, whereas the equivalent loop in WntD is much shorter and contains six disordered resides (Figures 2C and S1).

An unusual feature of the WntD NTD-linker structure is the presence of a 600 $Å^3$ solvent-filled cavity between helices A, B, C, D, and E (Figures 3A and 3B). The buried water molecules form hydrogen bonds largely with backbone atoms and with each other. XWnt8 also has a cavity in the corresponding region, but it is much narrower, with a volume of ~200 $Å^3$, and a Zn^{2+} is present one side of the cavity (Figure 3A). The less compact and larger solvent accessible core of WntD arises from outward displacements of helices A, C, D, and E relative to those of XWnt8 (Figure 2B). Helix B also sits in a different position relative to the other helices, and this feature, along with the shorter helix D, produces an open channel accessible to solvent molecules (Figures 2B and 3A). There are three entry paths for solvent

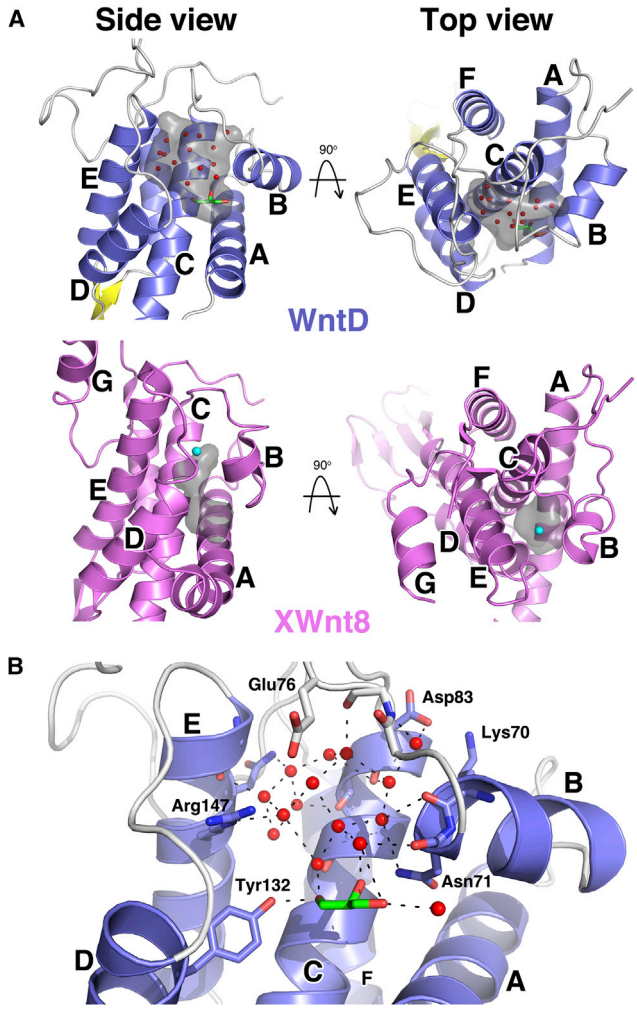

Figure 3. A Large Solvent-Accessible Cavity in WntD

(A) Surface representation (gray) of cavities inside the NTD α-helical cores of WntD (blue, top figure) and XWnt8 (magenta, bottom figure) as viewed from the side and the top. The water molecules and a glycerol molecule in the large cavity of WntD are shown in red spheres and green sticks, respectively. A Zn^{2+} (cyan sphere) is present on the top of the small cavity of XWnt8.

(B) Closeup of the solvent molecules in the large solvent-filled cavity of WntD. The hydrogen bond network within the WntD cavity is shown with dashed lines and the side chains and backbones of the water/glycerol-interacting residues are depicted as sticks. The entry paths of the solvent molecules are gated by three pairs of polar residues (sticks): Asn71/Tyr132, Glu76/Arg147, and Lys70/Asp83.

molecules. The first is at the front near Asn71 and Tyr132, between helices B and D. There are two others near the top of the molecule: one by Glu76 and Arg147, and the other near Lys70 and Asp83 (Figure 3B).

Linker Region Connecting the NTD and CTD of Wnt3a Is an LRP6 Binding Site

Purified Wnt3a, Fzd8, and LRP6 can form a ternary complex (Bourhis et al., 2010), indicating that Wnts use a distinct surface for interacting with its two coreceptors. Not all Wnt proteins signal through β-catenin or bind to LRP5/6, indicating that a variable region contributes to this interaction. One of the least conserved regions in the Wnt family is the linker that connects the NTD to the CTD. This region starts and ends with several conserved residues that form the interface between the two domains, but the intervening sequence is highly variable, including the large insertion of this linker region in *Wg* (Figure S1). In XWnt8, this region contains 13 disordered residues, but also includes another α helix (helix G, Figure 2D). Given that the linker is not conserved and is spatially distinct from the Fzd binding sites, we hypothesized that LRP5/6 binds to this flexible linker of certain Wnt proteins. Importantly, WntD does not interact genetically (Gordon et al., 2005) or physically (data not shown) with *Drosophila* Arrow, the LRP6 homolog. Moreover, although the WntD linker follows a remarkably similar path to that of XWnt8, it is shorter and well ordered (Figure 2D).

The extracellular region of LRP5/6 contains four repeating units of a β propeller and an EGF-like domain. Crystal structures of an LRP6 fragment spanning the third and fourth repeats (LRP6(3-4)) bound to the secreted Wnt inhibitor Dkk1, together with the analysis of charge reversal mutations, indicate that Dkk1 and Wnt3a bind to an overlapping surface of the LRP6 β propeller 3 (Ahn et al., 2011; Chen et al., 2011; Cheng et al., 2011; Bourhis et al., 2011). This surface is electrostatically negative, so we reasoned that the positively charged residues of the Wnt3a linker might contribute to LRP6 binding. Wnt3a contains three basic residues (Lys245, Arg247, and Arg250) at the beginning of the linker region; basic residues are also found in this region of XWnt8, which is disordered in the crystal structure (Figure S1). Two more basic residues (Arg257 and Arg259) are found in Wnt3a in positions corresponding to helix G of XWnt8, which contains a single basic residue (Arg235) at the beginning of the helix (Figures S1 and S5). Finally, Wnt3a contains two more basic residues, Lys264 and Arg269, in the C-terminal portion of the linker; these are absent in XWnt8 (Figure S1).

The contribution of positively charged Wnt3a linker residues to LRP6 binding was tested by charge reversal mutations. All mutant proteins were secreted (Figure S4A), suggesting that they were correctly processed. We further confirmed that purified wild-type and mutant Wnt3a proteins, including the NTD-linker truncation mutant, and the point mutations R250E, K245E/R247E/R250E, R257E/R259E, and K264E, bound to the cognate Fzd8 CRD with comparable affinities (Figure S4B). Because lipid modification is required for the interaction of the NTD with Fzd8 (Janda et al., 2012), these data indicate that the proteins are correctly modified and demonstrate that there is no overall structural disruption caused by point mutations in the flexible linker.

Using an autocrine Wnt reporter assay in HEK293T cells, we found that the Wnt3a mutations K245E and R247E had small or no effects on reporter activity, whereas R250E and the K245E/R247E/R250E triple mutations compromised activity (Figure 4A). Although the effect of R250E could be due to its reduced level of secretion (Figure S4A), similar protein levels of wild-type Wnt3a and the K245E/R247E/R250E triple mutant indicate that this basic region may contribute to LRP6 binding. R257E and R259E individually had small effects on Wnt3a signaling, but the R257E/R259E double mutant exhibited diminished activity (Figure 4A). In contrast, K264E, R269E and

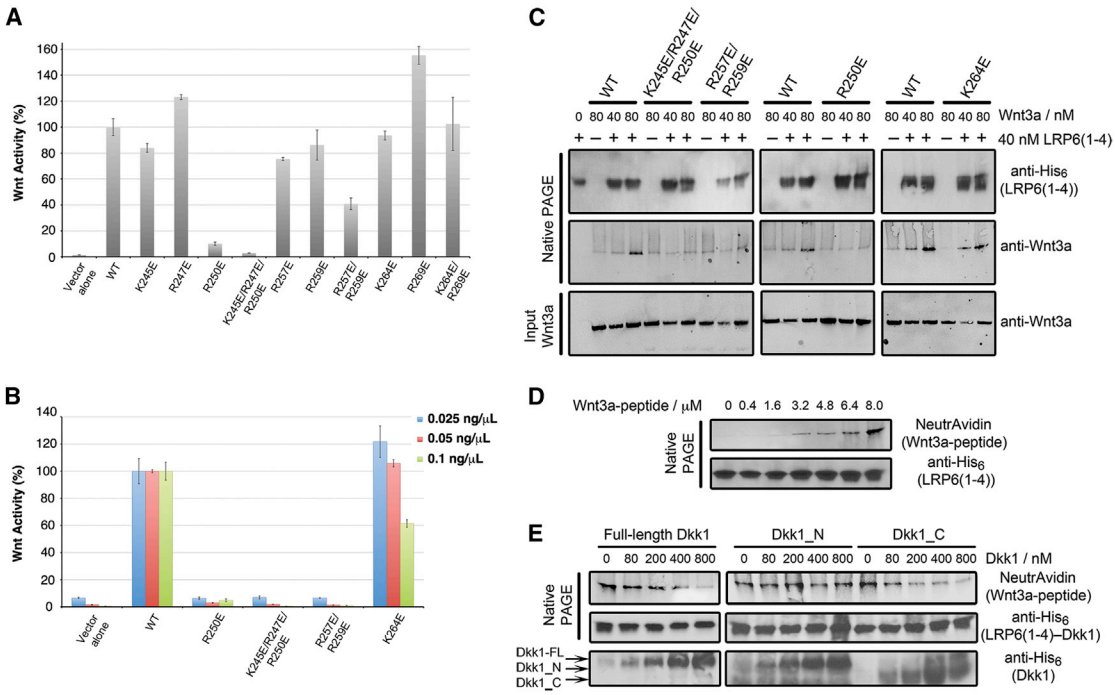

Figure 4. The NTD-CTD Linker Is Required for Wnt3a Activity and LRP6 Binding

(A) The effects of charge-reversal mutations on autocrine Wnt 3a reporter activity in HEK293T cells. Cells were transfected with 25 ng plasmid of the indicated mutants. Error bars denote standard deviation.

(B) Effect of Wnt3a linker mutations on paracrine Wnt3a reporter activity in LS/L reporter cells. Cells were treated with the indicated concentration of purified mutants. Error bars denote SD.

(C) Mutations in the linker affect Wnt3a binding to LRP6(1–4). Wnt3a mutants at indicated concentration were incubated with 40 nM LRP6(1–4), run on native PAGE, and analyzed by western blot with anti-His_6 (top) and anti-Wnt3a antibodies (middle). The highly basic Wnt3a protein or linker peptide (Figure 4D) cannot enter the gel unless it is bound to LRP6(1–4). The amount of input Wnt3a mutants in the gels was shown by running the same samples on a separate reducing SDS-PAGE, and analyzed by western blot with anti-Wnt3a antibody (bottom).

(D) Biotinylated Wnt3a linker peptide at the indicated concentration incubated with 80 nM LRP6(1–4), run on native PAGE, and analyzed by western blot with NeutrAvidin (top) and anti-His_6 antibody (bottom).

(E) Full-length Dkk1 and Dkk1_C, but not Dkk1_N can displace the peptide from LRP6(1–4). Eight micromolar Wnt3a peptide was incubated with 80 nM LRP6(1–4) and full-length Dkk1, Dkk1_N or Dkk1_C at the indicated concentration, run on native PAGE, and analyzed by western blot with NeutrAvidin (top) and anti-His_6 antibody (middle). The amount of input Dkk1 proteins in the gels was shown by running the same samples on a separate reducing SDS-PAGE, and analyzed by western blot with anti-His_6 antibody (bottom).

the double mutation K264E/R269E had little effect on reporter activity (Figure 4A), suggesting that the C terminus of the linker might not be involved in LRP6 binding.

To confirm the diminished activities of Wnt3a R250E, K245E/R247E/R250E, and the R257E/R259E mutants, the purified proteins were tested in a paracrine Wnt reporter assay using LS/L reporter cells (Figure 4B). None of these mutants stimulated the TOPFlash reporter, whereas the active mutant K264E behaved similarly to the wild-type Wnt3a. We next used native gel electrophoresis and western blot analysis to assess directly the LRP6-binding properties of the purified Wnt3a mutants (Figure 4C). Wild-type Wnt3a and K264E comigrated with a purified LRP6 extracellular fragment spanning the four repeats [LRP6(1–4)], consistent with their activities in the reporter assay. Conversely, R250E, the K245E/R247E/R250E triple mutant, and the R257E/R259E double mutant did not migrate with LRP6(1–4), indicating that these mutations significantly reduced or abolished LRP6 binding.

Although the Wnt3a mutants appear to be correctly folded and modified, we assayed the binding of a biotinylated synthetic peptide spanning residues 241–263 of Wnt3a to purified LRP6(1–4) to confirm that the linker region is directly involved in LRP6 binding. The peptide comigrated with LRP6(1–4) in a concentration-dependent manner (Figure 4D), whereas a Histone H2B peptide used as a control for nonspecific binding to a positively charged sequence did not (Figure S4C). Moreover, full-length Dkk1 and Dkk1_C, the C-terminal domain of Dkk1 that specifically binds to LRP6(3–4) (Ahn et al., 2011), but not Dkk1_N, displaced the peptide from LRP6(1–4) (Figure 4E), consistent with previous data demonstrating that LRP6(3–4) is the major binding site of Wnt3a (Bourhis et al., 2010) and that Wnt3a and Dkk1 bind to an overlapping, negatively charged surface of the LRP6 extracellular domain (Ahn et al., 2011).

DISCUSSION

Our data indicate that the Wnt3a NTD-CTD linker region is required for LRP6 binding and Wnt/β-catenin signaling activity. The linker sequence varies greatly among Wnt family members and thus might contribute to coreceptor specificity. We note,

however, that the linker may not be the only LRP6 binding site on Wnts because the binding affinity of the linker peptide appears to be substantially weaker than that on the Wnt3a protein (Figures 4C and 4D). This could be due to the increased entropy of the isolated peptide relative to its presence in the full-length protein. There may also be additional contacts formed by the partially conserved patch at the NTD-CTD interface proposed previously (Figure S5A; Janda et al., 2012), but these sites remain to be tested.

Although WntD does not signal through the Wnt/β-catenin pathway, the differences between the structure of its NTD-linker region and that of XWnt8 bound to the Fzd8 CRD offer insights into the interactions of Wnts and their binding partners. In XWnt8, the lipid protrudes from the tip of the E–F hairpin and binds into a hydrophobic groove on the Fzd CRD. In the uncomplexed WntD, this hairpin is shifted toward the direction of the "palm" formed by the α-helical core of the NTD. This position is consistent with the proposal that in the absence of Fzd, the E–F hairpin loop may form a fist so that the lipid might be protected from the aqueous environment (Willert and Nusse, 2012).

The β hairpins that connect helices C and D, and E and F, form a continuous β sheet structure in XWnt8. The tip of the E–F hairpin is modified by fatty acylation, and this region interacts directly with the Fzd8 CRD. In contrast, the loop connecting helices C and D is largely disordered in WntD, and the nonacylated E–F hairpin adopts a different spatial position with respect to that of the bound XWnt8. Although the C–D hairpin does not contact Fzd8 in the XWnt8-Fzd8 structure, it is possible that it is stabilized indirectly through its association with the E–F hairpin. It is interesting to speculate that the C–D hairpin, which includes several highly conserved residues, might be important for recognition by the acyltransferase responsible for the lipid modification of the E–F hairpin.

Comparison of the helical core of the two Wnt structures supports their proposed evolutionary relationships to saposin-like proteins (Bazan et al., 2012). Consistent with the results of Bazan and colleagues, the DALI algorithm (Holm and Rosenström, 2010) identifies saposin-like protein 1 (PDB 3S64) as one of the closest structural homologs of the WntD NTD (Z score = 3.0, Cα root-mean-square deviation [rmsd] = 2.7 Å). Saposin-like proteins comprise a four-helix bundle fold similar to that adopted by Wnt helices C–F (Figure S5B). Interestingly, the positions of helix B of WntD are quite different, consistent with the notion that helices A and B might be N-terminal additions to the ancient saposin-like core. Saposins are thought to undergo a major conformational rearrangement in which the two halves of the bundle separate to enable lipid binding, and it has been noted that saposin-like proteins have relatively loosely packed cores that might be important for enabling such changes (Anderson et al., 2003). There is no evidence that Wnt proteins undergo this change (which would probably be prevented by helices A and B), however, and the loose packing and presence of substantial cavities in WntD and XWnt8 may simply reflect the evolutionary relatedness of Wnts and saposin-like proteins.

A relatively large number of water molecules are found in the large WntD NTD cavity. XWnt8 has a more compact arrangement of its helical domain and thus has a smaller solvent-accessible volume, but might also contain solvent molecules that could not be visualized due to the limited resolution of that structure. We speculate that these cavities enable conformational plasticity of the helical bundle because there are fewer steric barriers to changing the relative positions of helices than in a closely packed hydrophobic core. Indeed, a similar water-filled cavity is a feature of conformationally complex G protein coupled receptors, which have different conformations associated with different activity states (Rosenbaum et al., 2007). Changes in the dispositions of the helices might enable changes in the relative positions of receptor-binding loops and β hairpins and thereby underlie the ability of several Wnt proteins to engage a given Fzd receptor, and conversely, the ability of a given Wnt to bind to more than one Fzd. Such plasticity might also be important for the ability to simultaneously engage different coreceptors. If so, the cavity could be a novel target for drugs that selectively stabilize or inhibit a particular Wnt-stimulated signaling pathway.

EXPERIMENTAL PROCEDURES

Protein Expression and Purification

Drosophila melanogaster Schneider 2 (S2) cells were stably transfected with a *Drosophila* WntD construct comprising the mature WntD sequence (residues 17–309) and an N-terminal Flag tag. Full-length WntD was purified using blue Sepharose (GE Healthcare), followed by anti-Flag M1 Agarose Affinity Gel (Sigma) and a HiTrap Heparin cation exchange column (GE Healthcare). Although full-length WntD was reported to be stable in the absence of detergent (Ching et al., 2008), initial attempts to concentrate it in the absence of detergents or with the commonly used detergent CHAPS was not successful. After screening 20 different detergents, we found that WntD could be concentrated up to 6 mg/ml in 0.5% (w/v) n-octyl-β-D-maltoside (Anatrace).

The NTD-linker fragment was cloned into the pMT/BiP/V5-His A expression vector (Life Technologies) to allow a hexa-histidine tag at the C terminus of the expressed proteins. Stable cell lines expressing WntD NTD-linker were produced by cotreansfecting the corresponding plasmid with pCoBlast selection vector (Life Technologies) into S2 cells using Cellfectin II Reagent (Life Technologies) according to the manufacturer's protocol. Stably transfected S2 cells were selected for 2 weeks with Schneider's insect medium (Sigma) supplemented with L-glutamine, 10% (v/v) heat-inactivated fetal bovine serum (FBS, Sigma), 100 units/ml penicillin, 100 μg/ml streptomycin, and 25 μg/ml Blasticidin S HCl (Life Technologies). Cells were maintained in the same medium and expanded to growth in 850-cm^2 roller bottles for large-scale protein production.

Expression of WntD NTD-linker was induced with 700 μM $CuSO_4$ at a cell density of 2 × 10^6 cells/ml. Conditioned medium was harvested after 5 days and centrifuged to remove cell debris. Supernatant was adjusted to 5 mM $CaCl_2$, 1 mM $NiSO_4$, 50 mM Tris (pH 8.0), and filtered and loaded onto an Ni^{2+}-NTA agarose column (QIAGEN). Resin was washed with ten column volumes of 50 mM Tris (pH 8.0), 1 M NaCl, and 20 mM imidazole and then two column volumes of 25 mM HEPES (pH 7.5), 300 mM NaCl, and 0.1% (w/v) n-Octyl-β-D-maltoside. Proteins were then eluted with the same buffer supplemented with 500 mM imidazole. The proteins were subsequently purified on MonoQ (GE Healthcare), and two distinct peak fractions that contained either the WntD NTD-linker monomer or a disulfide-linked dimer were eluted with a stepwise NaCl gradient with 25 mM HEPES (pH 7.5) and 0.1% (w/v) n-Octyl-β-D-maltoside. The monomeric WntD NTD-linker fractions were then treated with 1 mM iodoacetic acid (Sigma) two times, for 1 hr each on ice, to alkylate potential reactive cysteine(s) that cause disulfide-mediated dimerization or aggregation. The iodoacetic acid-treated monomeric proteins were further purified by gel filtration on Superdex 200 (GE Healthcare), respectively, in 25 mM HEPES (pH 7.5), 200 mM NaCl, and 0.1% (w/v) n-Octyl-β-D-maltoside. Purified WntD NTD-linker proteins were concentrated to 10–13 mg/ml for crystallization trials.

Crystallization and Data Collection

Small crystals of WntD NTD-linker monomer were initially grown by sitting drop vapor diffusion at 4°C, using equal volumes of protein and a reservoir solution

containing 20% (w/v) PEG1000, 100 mM Bis-Tris (pH 5.5), and 200 mM $MgCl_2$. A single crystal was crushed in the same reservoir solution using the Seed Bead kit (Hampton Research). Streak seeding was performed in pre-equilibrated drops of equal volumes of protein and a new reservoir solution containing 18% (w/v) PEG1000, 100 mM Bis-Tris (pH 5.5), and 200 mM $MgCl_2$ at both 4°C and 10°C. Crystals were transferred stepwise into a cryoprotectant buffer consisting of the reservoir solution containing up to 20% (v/v) glycerol from 5% (v/v) glycerol, and flash-frozen in liquid nitrogen. The diffraction data used for molecular replacement phasing and refinement, were from a single crystal grown at 10°C. A total of 360° of data were measured in 0.2° frames, using the PILATUS 6M detector on beamline 11-1 of the Stanford Synchrotron Radiation Laboratory (SSRL). Data were measured at 100 K at a wavelength of 0.98 Å. Data were indexed and integrated with XDS (Kabsch, 2010) and scaled using Scala (Evans, 2006). Data processing statistics are summarized in Table 1.

Structure Determination and Refinement

Initial phases were obtained by molecular replacement with PHASER (McCoy et al., 2007), using the crystal structure of the XWnt8 N-terminal domain (residues 35–268) (Protein Data Bank [PDB] accession number 4F0A) (Janda et al., 2012) with the interhelical loops and the two long β hairpins removed. Phases were further improved using solvent flipping and density truncation by density modification in CNS (Brünger et al., 1998) at 2.5 Å resolution. The model was built manually with Coot (Emsley and Cowtan, 2004) and refined with Phenix (Adams et al., 2002). After several rounds of refinement, interpretable electron density for most of the missing loops and a pair of long antiparallel β strands became evident, and the structure was refined to 2.1 Å. Although the crystallized material had been treated with iodoacetic acid, the single free cysteine (Cys232) appears to be unmodified. The geometry of the final model was validated using MolProbity (Chen et al., 2010). All structural figures were prepared with PyMOL (Schrodinger, 2010). Solvent-accessible cavities were analyzed using CASTp (Dundas et al., 2006), and electrostatic potential was calculated using APBS (Baker et al., 2001). The final refinement statistics are summarized in Table 1.

Cell Culture, Transfections, and Purification of Wnt3a Mutants

A mouse L-cell line stably transfected with SuperTOPFlash and LacZ expression constructs (LS/L reporter cells), L-Wnt3a (Willert et al., 2003) and HEK293T cells were routinely cultured in DMEM supplemented with L-glutamine, 10% (v/v) FBS, 100 units/ml penicillin, and 100 μg/ml streptomycin (Life Technologies), in a 5% CO_2 humidified atmosphere at 37°C.

Full-length mouse Wnt3a and Wnt3a NTD-linker (residues 1–280) were cloned into the pcDNA3.1(+)/myc-His B vector (Life Technologies) between *BamH*I and *Age*I restriction sites, respectively, and a stop codon was introduced after the Wnt3a sequences to avoid the C-terminal hexa-histidine tag. Full-length Wnt3a mutants were generated by site-directed mutagenesis.

To produce purified Wnt3a NTD-linker, full-length wild-type and mutant proteins, HEK293T cells were seeded in 100 mm^2 cell culture dishes in DMEM containing 10% (v/v) FBS for overnight. Cells were then transiently transfected with the Wnt3a plasmids using Lipofectamine 2000 (Life Technologies) according to the manufacturer's protocol. The media were replaced with fresh DMEM growth media after 6 hr. The conditioned media were harvested at 48 hr posttransfection, filtered, CHAPS (Sigma) was added to the final 1% (w/v) concentration, mixed with blue sepharose beads, and incubated overnight at 4°C. The beads were washed with ten column volumes of 20 mM Tris (pH 7.5), 150 mM KCl, and 1% (w/v) CHAPS, and the proteins were eluted with the same buffer supplemented with 1.5 M KCl and dialyzed against 1× PBS with 1% (w/v) CHAPS for overnight at 4°C. The concentrations of these partially purified Wnt3a proteins were estimated by comparing the band intensity of a purified mouse Wnt3a protein (StemRD) at known concentration in western blots using mouse anti-Wnt3a antibodies (Santa Cruz Biotechnology) and IRDye 800CW conjugated antimouse secondary antibodies (Li-Cor).

Wnt Signaling Assays

The activities of Wnt3a mutants were first tested using an autocrine Wnt-responsive TOPFlash luciferase reporter assay by transient expression in HEK293T cells. HEK293T cells were seeded in 96-well plates in DMEM containing 10% (v/v) FBS. After 6 hr, cells were transiently cotransfected with the SuperTOPFlash and LacZ expression plasmids, as well as the indicated Wnt3a mutants, using Lipofectamine 2000 according to the manufacturer's protocol. The media were replaced with fresh DMEM growth media at 18 hr posttransfection. After another 18 hr, Luciferase reporter activity was measured in a Veritas Luminometer (Turner Biosystems). Assays were carried out in triplicate, and relative luciferase units were normalized to LacZ.

For those transiently expressed Wnt3a mutants showing dramatic decrease in TOPFlash activity in HEK293T cells, the activities of equal amount of purified mutant proteins were also examined in the LS/L reporter cells in a paracrine activity assay. Luciferase reporter activity was measured in the Veritas Luminometer. Assays were carried out in triplicate, and relative luciferase units were normalized to LacZ.

Native PAGE Binding Assays

Human LRP6(1–4) (residues 21–1246), full-length Dkk1 (residues 31–266), Dkk1_N (residues 31–142), and Dkk1_C (residues 178–266) were expressed as histidine-tagged proteins and purified from *Sf*9 cells as previously described (Ahn et al., 2011). The Wnt3a linker peptide (residues 241–263) was biotinylated at the N terminus with 6-aminohexanoate (LC) as a spacer and amidated at the C terminus during synthesis (Anaspec). For the binding between Wnt3a mutants and LRP6(1–4), purified proteins were incubated for 1 hr at room temperature. For the binding between the Wnt3a linker peptide and LRP6(1–4) with or without Dkk1, purified proteins were incubated for 1 hr at room temperature or overnight at 4°C. Samples were then run on native PAGE as previously described (Ahn et al., 2011). Proteins were transferred to nitrocellulose membranes and analyzed by western blotting with anti-Wnt3a antibodies for the detection of Wnt3a proteins or with DyLight 800 Dye-conjugated NeutrAvidin (Pierce) for the detection of the biotinylated peptide. To detect the LRP6(1–4) proteins, the same membranes were washed by Restore PLUS western blot stripping buffer (Thermal Scientific) and reprobed with anti-His_6 HRP conjugated antibodies (QIAGEN). To detect Wnt3a and Dkk1 proteins, the same samples were run in a separate reducing SDS-PAGE gel and analyzed by western blotting with anti-Wnt3a antibodies and anti-His_6 HRP conjugated antibodies, respectively.

ACCESSION NUMBERS

The PDB accession number for the coordinates and structure factors for the WntD NTD-linker is 4KRR.

SUPPLEMENTAL INFORMATION

Supplemental Information includes five figures and can be found with this article online at http://dx.doi.org/10.1016/j.str.2013.05.006.

ACKNOWLEDGMENTS

We thank Denise Tran, Thulashitha Rajasingham, and Matthew Fish for technical assistance, Tzanko Doukov (Stanford Synchrotron Radiation Lightsource [SSRL]) for beamline support, and Terence Hui (ForteBio) for Octet system support. M.L.-H.C. was supported by a postdoctoral fellowship from the American Heart Association. This work was supported by U.S. National Institutes of Health grants AG33596 and AG39420 (to W.I.W.). Portions of this research were carried out at the SSRL, which is supported by the U.S. Department of Energy and the National Institutes of Health. M.L.-H.C. modified the WntD purification and performed all other experiments and data analysis; V.E.A. and D.L.D. developed the initial full-length WntD expression and purification procedures; H.-J.C. performed molecular replacement phasing and initial refinement; R.N. advised on initial purification of WntD and revised the manuscript; and W.I.W. oversaw all the experiments and wrote the paper with M.L.-H.C.

Received: March 19, 2013
Revised: May 3, 2013
Accepted: May 14, 2013
Published: June 20, 2013

REFERENCES

Adams, P.D., Grosse-Kunstleve, R.W., Hung, L.W., Ioerger, T.R., McCoy, A.J., Moriarty, N.W., Read, R.J., Sacchettini, J.C., Sauter, N.K., and Terwilliger, T.C. (2002). PHENIX: building new software for automated crystallographic structure determination. Acta Crystallogr. D Biol. Crystallogr. *58*, 1948–1954.

Ahn, V.E., Chu, M.L., Choi, H.J., Tran, D., Abo, A., and Weis, W.I. (2011). Structural basis of Wnt signaling inhibition by Dickkopf binding to LRP5/6. Dev. Cell *21*, 862–873.

Anderson, D.H., Sawaya, M.R., Cascio, D., Ernst, W., Modlin, R., Krensky, A., and Eisenberg, D. (2003). Granulysin crystal structure and a structure-derived lytic mechanism. J. Mol. Biol. *325*, 355–365.

Baker, N.A., Sept, D., Joseph, S., Holst, M.J., and McCammon, J.A. (2001). Electrostatics of nanosystems: application to microtubules and the ribosome. Proc. Natl. Acad. Sci. USA *98*, 10037–10041.

Bazan, J.F., Janda, C.Y., and Garcia, K.C. (2012). Structural architecture and functional evolution of Wnts. Dev. Cell *23*, 227–232.

Bejsovec, A., and Wieschaus, E. (1995). Signaling activities of the Drosophila wingless gene are separately mutable and appear to be transduced at the cell surface. Genetics *139*, 309–320.

Bourhis, E., Tam, C., Franke, Y., Bazan, J.F., Ernst, J., Hwang, J., Costa, M., Cochran, A.G., and Hannoush, R.N. (2010). Reconstitution of a frizzled8.Wnt3a.LRP6 signaling complex reveals multiple Wnt and Dkk1 binding sites on LRP6. J. Biol. Chem. *285*, 9172–9179.

Bourhis, E., Wang, W., Tam, C., Hwang, J., Zhang, Y., Spittler, D., Huang, O.W., Gong, Y., Estevez, A., Zilberleyb, I., et al. (2011). Wnt antagonists bind through a short peptide to the first β-propeller domain of LRP5/6. Structure *19*, 1433–1442.

Brünger, A.T., Adams, P.D., Clore, G.M., DeLano, W.L., Gros, P., Grosse-Kunstleve, R.W., Jiang, J.S., Kuszewski, J., Nilges, M., Pannu, N.S., et al. (1998). Crystallography & NMR system: A new software suite for macromolecular structure determination. Acta Crystallogr. D Biol. Crystallogr. *54*, 905–921.

Chen, V.B., Arendall, W.B., 3rd, Headd, J.J., Keedy, D.A., Immormino, R.M., Kapral, G.J., Murray, L.W., Richardson, J.S., and Richardson, D.C. (2010). MolProbity: all-atom structure validation for macromolecular crystallography. Acta Crystallogr. D Biol. Crystallogr. *66*, 12–21.

Chen, S., Bubeck, D., MacDonald, B.T., Liang, W.X., Mao, J.H., Malinauskas, T., Llorca, O., Aricescu, A.R., Siebold, C., He, X., and Jones, E.Y. (2011). Structural and functional studies of LRP6 ectodomain reveal a platform for Wnt signaling. Dev. Cell *21*, 848–861.

Cheng, Z., Biechele, T., Wei, Z., Morrone, S., Moon, R.T., Wang, L., and Xu, W. (2011). Crystal structures of the extracellular domain of LRP6 and its complex with DKK1. Nat. Struct. Mol. Biol. *18*, 1204–1210.

Ching, W., Hang, H.C., and Nusse, R. (2008). Lipid-independent secretion of a Drosophila Wnt protein. J. Biol. Chem. *283*, 17092–17098.

Couso, J.P., and Martinez Arias, A. (1994). Notch is required for wingless signaling in the epidermis of Drosophila. Cell *79*, 259–272.

Dundas, J., Ouyang, Z., Tseng, J., Binkowski, A., Turpaz, Y., and Liang, J. (2006). CASTp: computed atlas of surface topography of proteins with structural and topographical mapping of functionally annotated residues. Nucleic Acids Res. *34*(Web Server issue), W116–W118.

Emsley, P., and Cowtan, K. (2004). Coot: model-building tools for molecular graphics. Acta Crystallogr. D Biol. Crystallogr. *60*, 2126–2132.

Evans, P. (2006). Scaling and assessment of data quality. Acta Crystallogr. D Biol. Crystallogr. *62*, 72–82.

Ganguly, A., Jiang, J., and Ip, Y.T. (2005). Drosophila WntD is a target and an inhibitor of the Dorsal/Twist/Snail network in the gastrulating embryo. Development *132*, 3419–3429.

Gordon, M.D., Dionne, M.S., Schneider, D.S., and Nusse, R. (2005). WntD is a feedback inhibitor of Dorsal/NF-kappaB in Drosophila development and immunity. Nature *437*, 746–749.

Holm, L., and Rosenström, P. (2010). Dali server: conservation mapping in 3D. Nucleic Acids Res. *38*(Web Server issue), W545–W549.

Hoppler, S., Brown, J.D., and Moon, R.T. (1996). Expression of a dominant-negative Wnt blocks induction of MyoD in Xenopus embryos. Genes Dev. *10*, 2805–2817.

Janda, C.Y., Waghray, D., Levin, A.M., Thomas, C., and Garcia, K.C. (2012). Structural basis of Wnt recognition by Frizzled. Science *337*, 59–64.

Kabsch, W. (2010). Integration, scaling, space-group assignment and post-refinement. Acta Crystallogr. D Biol. Crystallogr. *66*, 133–144.

MacDonald, B.T., Tamai, K., and He, X. (2009). Wnt/beta-catenin signaling: components, mechanisms, and diseases. Dev. Cell *17*, 9–26.

McCoy, A.J., Grosse-Kunstleve, R.W., Adams, P.D., Winn, M.D., Storoni, L.C., and Read, R.J. (2007). Phaser crystallographic software. J. Appl. Cryst. *40*, 658–674.

McElwain, M.A., Ko, D.C., Gordon, M.D., Fyrst, H., Saba, J.D., and Nusse, R. (2011). A suppressor/enhancer screen in Drosophila reveals a role for wnt-mediated lipid metabolism in primordial germ cell migration. PLoS ONE *6*, e26993.

Rosenbaum, D.M., Cherezov, V., Hanson, M.A., Rasmussen, S.G., Thian, F.S., Kobilka, T.S., Choi, H.J., Yao, X.J., Weis, W.I., Stevens, R.C., and Kobilka, B.K. (2007). GPCR engineering yields high-resolution structural insights into beta2-adrenergic receptor function. Science *318*, 1266–1273.

Schrodinger. (2010). The PyMOL Molecular Graphics System, Version 1.3r1.

Takada, R., Satomi, Y., Kurata, T., Ueno, N., Norioka, S., Kondoh, H., Takao, T., and Takada, S. (2006). Monounsaturated fatty acid modification of Wnt protein: its role in Wnt secretion. Dev. Cell *11*, 791–801.

Willert, K., and Nusse, R. (2012). Wnt proteins. Cold Spring Harb. Perspect. Biol. *4*, a007864.

Willert, K., Brown, J.D., Danenberg, E., Duncan, A.W., Weissman, I.L., Reya, T., Yates, J.R., 3rd, and Nusse, R. (2003). Wnt proteins are lipid-modified and can act as stem cell growth factors. Nature *423*, 448–452.

Wu, C.H., and Nusse, R. (2002). Ligand receptor interactions in the Wnt signaling pathway in Drosophila. J. Biol. Chem. *277*, 41762–41769.

